NANO LETTERS

2004
Vol. 4, No. 7
1197−1201

Imperfect Oriented Attachment: Accretion and Defect Generation of Nanosize Rutile Condensates

M. H. Tsai,[†] S. Y. Chen,*[,‡] and P. Shen[†]

Institute of Materials Science and Engineering, National Sun Yat-sen University, Kaohsiung, Taiwan, R.O.C., and Department of Mechanical Engineering, I-Shou University, Kaohsiung, Taiwan, R.O.C.

Received March 16, 2004; Revised Manuscript Received May 30, 2004

ABSTRACT

Imperfect oriented attachment of nanoparticles over specific surfaces is rationalized to cause accretion and defects for the rutile condensates. Analytical electron microscopy indicates that rutile nanoparticles prepared by Nd:YAG laser ablation on Ti targets have well-developed {110} and {011} surfaces with steps. These surfaces are beneficial to {∼110} and {∼011} vicinal attachment, causing, respectively, edge dislocations and planar defects, i.e., fault and twin for rutile crystal. The {011}-interface relaxation, by shearing along ⟨011⟩ directions, accounts for a rather high density of edge dislocations near the planar defects thus formed. Brownian motion may proceed above a critical temperature for anchorage release at the interface of imperfect attached nanoparticles until an epitaxial relationship is reached.

A crystal in terms of 2-D assembly of liquid crystals (e.g., inorganic-encased hexagonal mesophase with plane group *P*6*mm*)[1] or 3-D ordering of atoms (e.g., TiO_2 in the anatase form with space group *I*4/*amd*)[2] in colloidal hydrothermal solution was recently proved to generate dislocations by imperfect oriented attachment on a specific atomic plane of nanoparticles, whereas twin boundaries or another planar defect are caused via oriented attachment on such planes.[3] The fluorite-type condensates with fcc-type stacking sequences, such as CeO_2 prepared by laser ablation condensation, were also shown to be twinned by coalescence over a specific {111} contact plane.[4] As for TiO_2 condensate in the rutile form (space group $P4_2/mnm$), a semiconductor photocatalyst with selective activity toward certain substrates,[5] it was not previously realized to have specific low-energy surfaces for analogous attachments.

In this report we describe accretion and defect generation of rutile condensates in terms of attachment over specific surfaces of nanoparticles. This view is based on the scrutiny of the defects and shape of the rutile nanoparticles prepared by a laser ablation condensation route. We suggest that, regardless of the coexistence of other polymorphs, the rutile condensates once formed may accrete by Brownian motion and reorient/shear impinged nanoparticles until an energetically favored state is reached.

Nd:YAG laser (JK laser, 1.06 μm in wavelength, beam mode: TEM00) pulse irradiation (2 J/pulse) was employed at a specified pulse time duration (2.4 ms at 30 Hz), spot size (0.146 mm^2) and oxygen flow rate (6 L/min) to vaporize a Ti target (99.999% purity). Under such conditions, the rutile nanoparticles that focus our attention prevailed along with anatase nanoparticles. (A higher oxygen flow rate (20 L/min) and optimum energy input (0.5 to 2 J/pulse) in our previous study has produced additional α-PbO_2-type TiO_2 particles,[6] which shed light on their possible condensation around stars in addition to terrestrial occurrences, e.g., as a response to static high pressure in crustal rocks attending subduction into Earth's interior[7] or as a response to natural dynamic events in shocked rocks from the crater.[8]) The condensates were collected on copper grids overlaid with a carbon-coated collodion film and fixed in position by a plastic holder at a distance of 2.5 mm from the target. Analytical electron microscopy (AEM) was used to characterize composition and crystal structures of the TiO_2 condensates using a JEOL 3010 instrument at 300 keV for imaging, selected area electron diffraction (SAED), and point-count energy-dispersive X-ray (EDX) analysis at a beam size of 10 nm. Two-dimensional Fourier transform and reconstructed lattice images were used to characterize the shape and defects as well as the coalescence behavior of the nanosize rutile particles.

The lattice image of a typical rutile nanoparticle in Figure 1a shows well-developed $(1\bar{1}0)$ lattice planes extending along the crystallographic *c*-axis, as confirmed by Fourier transform (Figure 1b) from the specified square region in Figure 1a.

* Corresponding author. FAX +886-7-6578853; E-mail: steven@isu.edu.tw.
[†] National Sun Yat-sen University.
[‡] I-Shou University.

10.1021/nl0495763 CCC: $27.50
Published on Web 06/22/2004

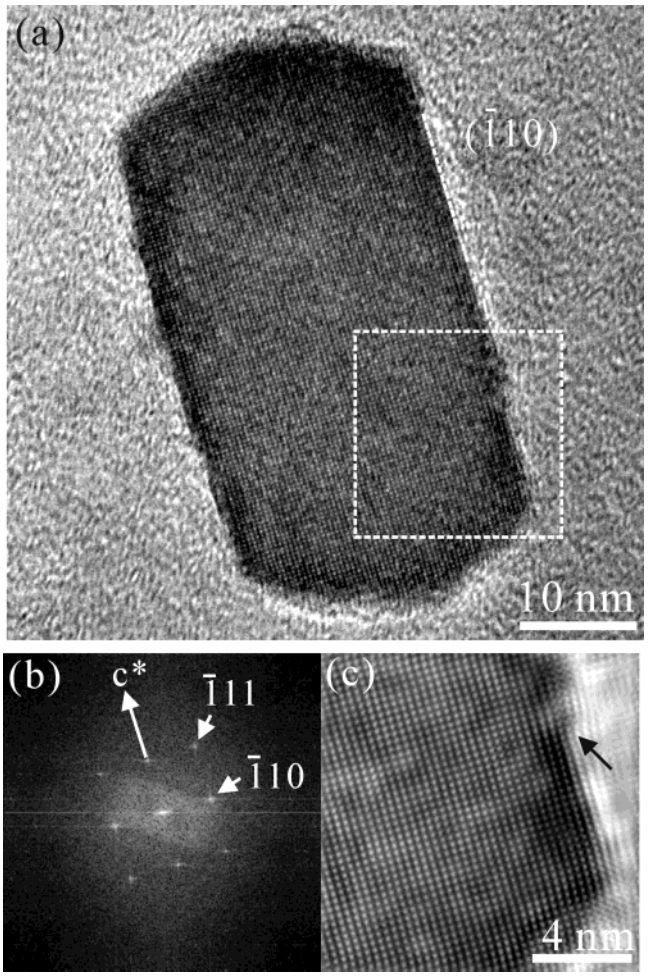

Figure 1. (a) Lattice image of a typical rutile nanoparticle in [110] zone axis showing a well-developed ($\bar{1}10$) surface extending along the crystallographic *c*-axis. (b) Fourier transform (reciprocal *c** axis and (*hkl*) labeled) and (c) reconstructed image from the square region in (a) showing a step (arrow) on the ($\bar{1}10$) surface and the dislocation-free interior. Sample prepared by laser ablation condensation at 2 J/pulse and an oxygen flow rate of 6 L/min.

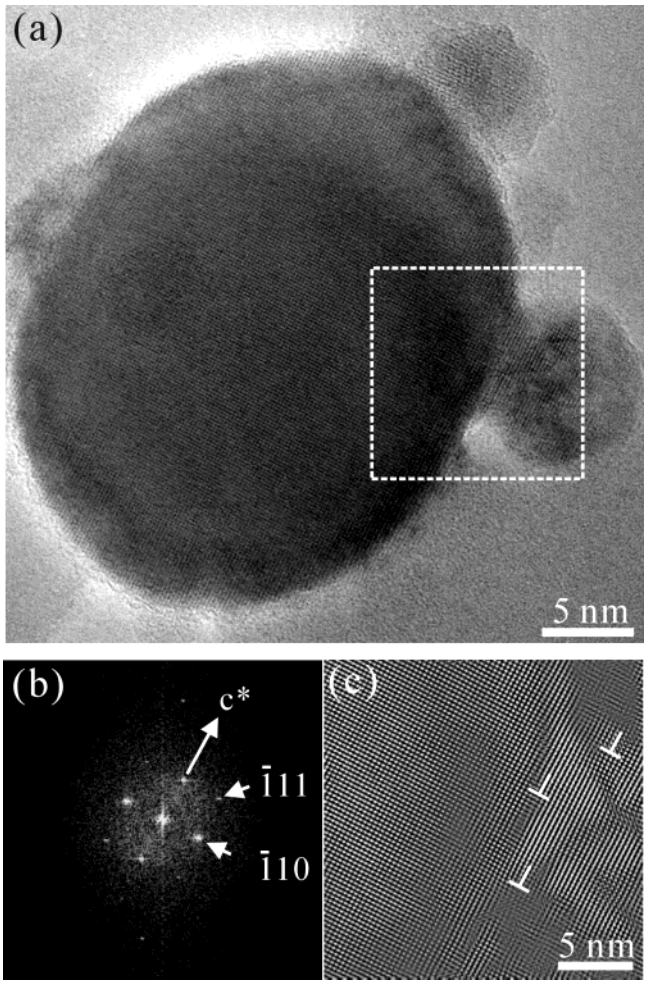

Figure 2. (a) Lattice image of two rutile nanoparticles coalesced over the ($\bar{1}10$) face into a single crystal in the [110] zone axis. (b) Fourier transform and (c) reconstructed image from the square region in (a) showing edge dislocations (denoted by T) at the interface and within the smaller particle.

The reconstructed image (Figure 1c) shows in further detail the step on the ($\bar{1}10$) surface and the dislocation-free interior. The {110} surface is in fact the most stable low-index nonpolar surface for rutile[9,10] and prevails in crustal rocks.[11] The rutile nanoparticles tended to impinge over the {∼110} vicinal surface to form a single crystal, yet with lattice imperfections (Figure 2). In such a case, edge dislocations having a half plane parallel to {110} occurred at the interface and within the relatively small particle (Figure 2).

The rutile nanoparticles also impinged over the {∼011} vicinal surface to form an extrinsic fault, i.e., insertion of one layer at a fault interface, (Figure 3) and a twin boundary (Figure 4). The {011} fault assigned as ($10\bar{1}$) in Figure 3a was truncated by a well-developed ($1\bar{1}0$) surface. Fourier transform (Figure 3b) and a reconstructed image (Figure 3c) from the fault showed further its termination by dislocations with a half plane parallel to the {$1\bar{1}0$} plane. The twinned bicrystals, with well-developed {110} and {011} surfaces (Figure 4a), were characterized by Fourier transform (Figure 4b) to follow the same twin law as the so-called geniculated twin commonly found in crustal rocks.[11] The reconstructed image covering the twin boundary (Figure 4c) showed primarily ($0\bar{1}1$) faults and dislocations with half planes parallel to ($\bar{1}10$). The fault and dislocation density are both decreasing away from the twin boundary as indicated by the Fourier transform (Figure 4d) and reconstructed image (Figure 4e) taken from one of the twin variants ca. 20 nm away from the twin boundary.

Rapid cooling of the condensates under the influence of oxygen background gas[6] may possibly cause crystal deformation and hence lattice imperfections. However, the fact that the dislocations are enriched near specific contact planes parallel to well-developed surfaces, implies an alternative mechanism of defect generation. We suggest that these planar defects were generated by imperfect attachment of the nanoparticles over their specified surfaces. Since the rutile nanoparticles have well developed {110} and {011} surfaces with steps, these surfaces are beneficial to {∼110} and {∼011} vicinal attachment to form specific defects, depending on the crystal symmetry and anchorage position of the contact plane as addressed in turn.

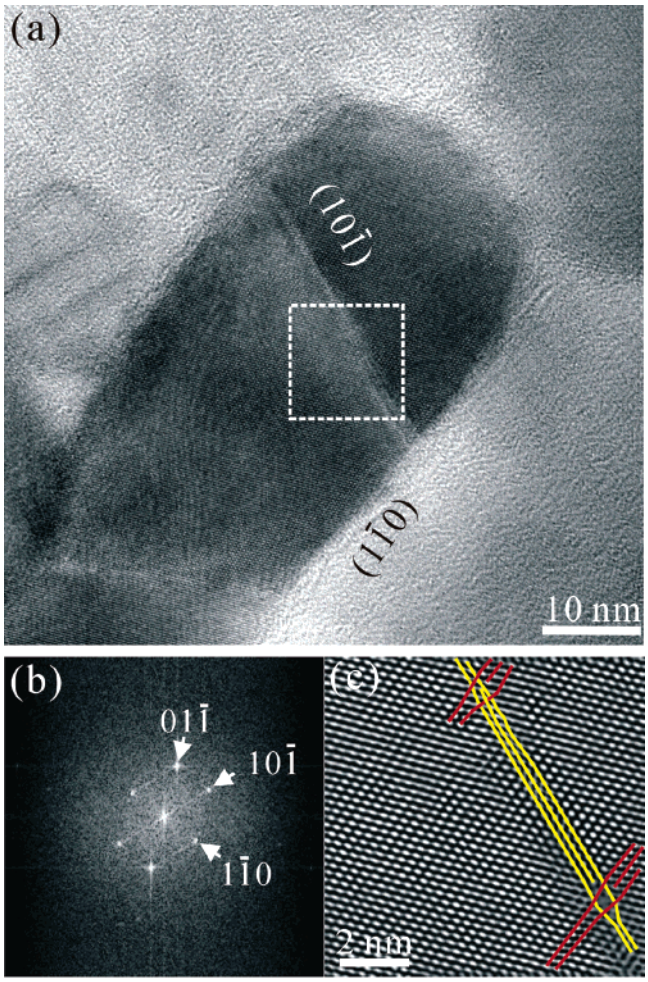

Figure 3. (a) Lattice image of two rutile nanoparticles coalesced over (10$\bar{1}$) to form the fault viewed in the [111] zone axis. (b) Fourier transform and (c) reconstructed image from the square region in (a) showing the fault plane parallel to (10$\bar{1}$) (delineated by yellow lines) and fault-terminating dislocations with half plane parallel to (1$\bar{1}$0) as delineated by red lines.

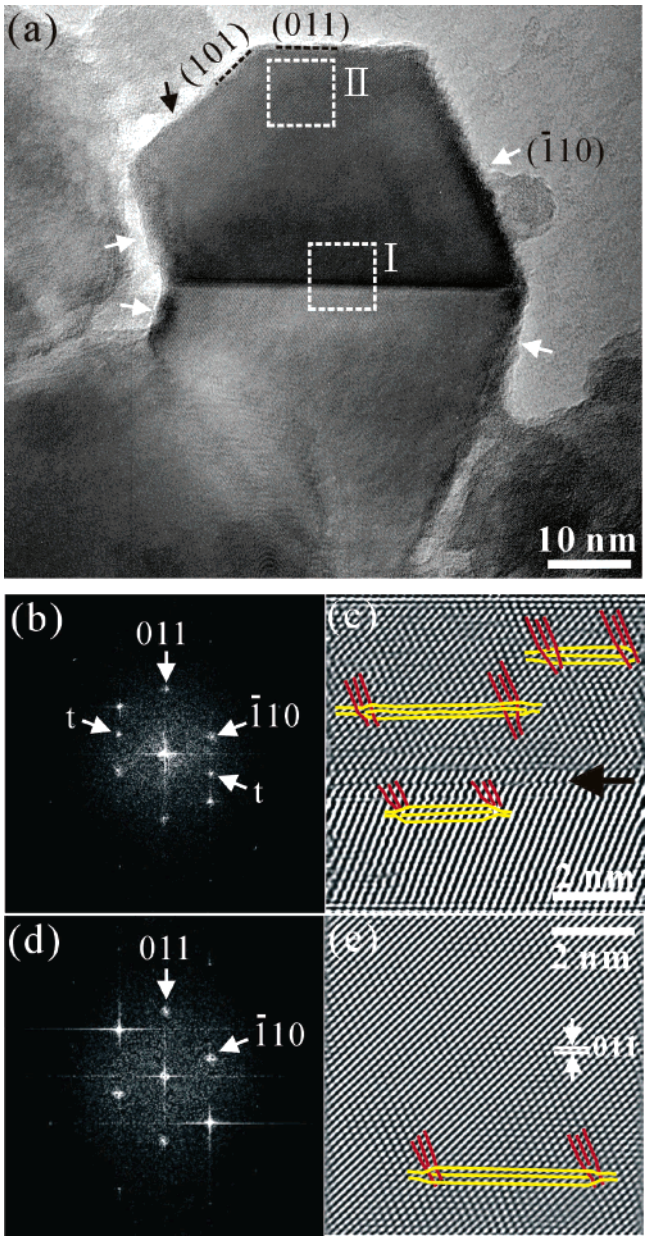

Figure 4. (a) Lattice image of two rutile nanoparticles coalesced over a specific (011) surface to form twinned bicrystals. The well-developed {110} surfaces are indicated by white arrows, whereas the step on the (101) surface is indicated by the dark arrow. (b) Fourier transform ([11$\bar{1}$] zone axis with (*hkl*) of one variant labeled and twinned spots denoted by the letter t) and (c) reconstructed image from the square region (I) in (a) showing the (011) fault (delineated by yellow lines) and dislocations with half plane parallel to (1$\bar{1}$0) (delineated by red lines) in the vicinity of the twin boundary denoted by an arrow. (d) and (e) Fourier transform and reconstructed image, respectively, for the square region (II) of the upper twin variant with many fewer defects.

Unification/twinning of impinged rutile particles apparently depends on the crystal symmetry of the contact plane. Having vertical mirror planes, either unrelaxed[12] or relaxed[13] (Figure 5a), the (110) surface is not allowed for coalescence twinning. By contrast, the (011) contact plane, with 2-fold rotation symmetry but no vertical mirror plane, either unrelaxed[12] or relaxed[13] (Figure 5b), is allowed for coalescence twinning analogous to the case of (111)-specific coalescence twinning for CeO_2 condensates.[4] A maximum of 60 degrees rotation over the (111) contact plane is required for the attached fluorite-type particles to be twinned or in parallel epitaxy.[4] However, in the present case of rutile crystallites adjoining over {011}, it needs to rotate within 90 degrees (cw or ccw) to be in parallel epitaxy or twinned, as depicted schematically with the {011} lattice planes edge-on in Figure 6a and 6b, respectively.

As for unification/faulting specification, it may depend on anchorage position at the (011) contact plane as depicted edge-on in Figure 6a vs 6c for intrinsic fault and 6d for extrinsic fault with two violations of the stacking rule. Translation for a specified displacement vector R of 0.5[0$\bar{1}$1] is a faulting or unification operation.[14] However, faulting with oxygen-terminated contact and $R \sim 0.25[0\bar{1}1]$ has also been suggested, based on convergent beam diffraction of deformed rutile crystals,[15] to have 8-coordinated Ti vacant sites (Figure 6e). Such an interface is not stable and may trigger shearing along the [0$\bar{1}$1] direction. It is also energetically favorable for the twin boundary (Figure 6b) and fault plane with $R = 0.5[011]$, either intrinsic (Figure 6c) or

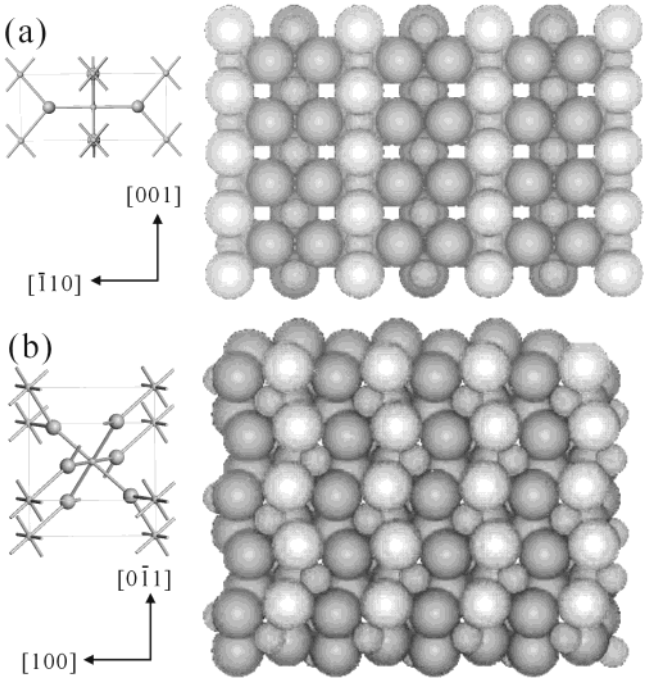

Figure 5. (a) The (110) projection of rutile lattice in unrelaxed[12] (left) and relaxed state[13] (right) showing two vertical mirror planes. (b) The (011) projection of rutile lattice in unrelaxed[12] (left) and relaxed state[13] (right) showing a 2-fold rotation plane normal and rows of oxygen ions aligned along the ($0\bar{1}04$) plane normal, i.e., [0$\bar{1}$1] direction, bonded to five-coordinate titanium ions.[13] Small and large circles (not to scale) denoted the Ti and oxygen atoms, respectively.

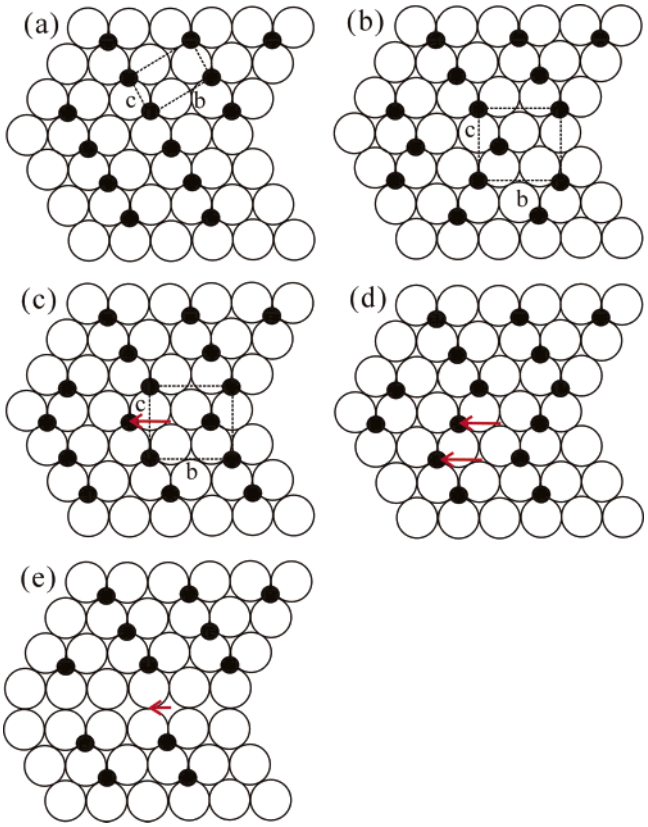

Figure 6. Schematic drawing of atom positions and crystallographic axes *b* and *c* for the rutile (*b* = *a* axis) crystals coalesced over (011) to form (a) single crystal, (b) twinned bicrystals, (c) intrinsic fault with $R = 0.5[0\bar{1}1]$, (d) extrinsic fault derived from (c) by a further slip with $R = 0.5[0\bar{1}1]$, (e) fault with $R \sim 0.25[0\bar{1}1]$. Small solid circles and large open circles denote the Ti and oxygen atoms, respectively. Note the basic unit of α-PbO_2-type TiO_2 (denoted by dotted cell) at planar defects for (b) and (c) and displacement vector *R* (denoted by an arrow) parallel to [0$\bar{1}$1] in (c), (d), and (e).

extrinsic (Figure 6d), to be sheared along [0$\bar{1}$1] so that the metastable α-PbO_2 type unit slab[7] can be relaxed. Interface relaxation via this shearing mechanism accounts for a high density of edge dislocations near the fault (Figure 3) and twin boundary (Figure 4). The attachment of an oxygen-terminated {011} surface or a {∼011} vicinal surface may also cause Ti diffusion for a more relaxed state at the interface.

The attachment over (110) and (011) may temporarily serve to reduce overall surface energy by eliminating the surfaces at which the rutile crystallites join. Thermodynamically, Brownian motion may still proceed above a critical temperature for anchorage release at the interface of imperfect attached particles until an epitaxial relationship is reached. This process is analogous to the case of {∼111} vicinal surface specific coalescence for CeO_2[17] and tetragonal ZrO_2[18] nanocondensates as inferred from fcc metal crystallites migrating and rotating on a single-crystal substrate, KCl(100), with or without steps. Experimentally, fcc metal crystallites have been proved to be able to migrate-rotate[19] and coalesce[20] on the free surface of single-crystal substrate, regardless of the presence of surface steps,[21] until low-energy epitaxial orientation with respect to the substrate was reached. (Refer to ref 22 for a retrospect of the experimental results and theoretical considerations of Brownian type rotation of nonepitaxial crystallites on single-crystal substrate.) Einstein's molecular theory of heat, Eyring's transition state model, and frictional force at a viscous interface were successfully adopted to formulate the diffusivity equation of the crystallite over the single-crystal substrate.[23,24] A critical temperature (T_c) must be reached for anchorage release and for the crystallites to move under a frictional force related to interfacial viscosity. It should be noted that nanosize Au particles have been proved to migrate-rotate and coalesce on a KCl(100) substrate at a rather low temperature (94 °C).[23] In the present laser ablation process, post-condensation radiant heating to around 900 °C is manifested by the occasional agglomeration of titania nanoparticles in a compact manner[25,26] in addition to nanochain aggregates, which tend to stretch under tension and contract when tension is relaxed.[27] At such a high temperature, Brownian motion of rutile nanoparticles can be readily activated until a parallel-epitaxial relationship or a secondary energy cusp for the twin boundary is reached.

We are proposing a mechanism for the growth and defect generation of the nanosize rutile condensates via their imperfect oriented attachment over {∼110} and {∼011} vicinal surfaces followed by Brownian motion of the adjoined nanoparticles until low-energy epitaxial orientation is reached. The {∼011} attachment derived fault or twin boundary was

alternatively relaxed by nearby shearing along ⟨011⟩ directions. This model is important if generalized to oxides with rutile-type isostructure formed in a natural condensation or dynamic event.

Acknowledgment. We thank L. Tseng for technical assistance on laser ablation, L. J. Wang for technical assistance on AEM, and an anonymous referee for constructive comments. Supported by Center for Nanoscience and Nanotechnology at NSYSU and National Science Council, Taiwan, R.O.C. under contracts NSC 91-2216-E−214-009 and NSC 92-2120-M-110-001.

References

(1) Shen, P.; Fahn, Y. Y.; Su, A. C. *Nano Lett.* **2001**, *1*, 299.
(2) Penn, R. L.; Banfield, J. F. *Science* **1998**, *281*, 969.
(3) Penn, R. L.; Banfield, J. F. *Am. Mineral.* **1998**, *83*, 1077.
(4) Lee, W. S.; Shen, P. *J. Cryst. Growth* **1999**, *205*, 169.
(5) Hoffmann, M. R.; Martin, S. T.; Choi, W.; Bahnemann, D. W. *Chem. Rev.* **1995**, *95*, 69.
(6) Chen, S. Y.; Shen, P. *Phys. Rev. Lett.* **2002**, *89*, 096106-1.
(7) Hwang, S. L.; Shen, P.; Chu, H. T.; Yui, T. F. *Science* **2000**, *288*, 321.
(8) El Goresy, A.; Chen, M.; Dubrovinsky, L.; Gillet, P.; Graup, G. *Science* **2001**, *293*, 1467.
(9) Henrich, V. E.; Cox, P. A. *The Surface Science of Metal Oxides*; Cambridge University Press: Cambridge, 1994; p 318.
(10) Gibson, A. S.; Lafemina, J. P. *Structure of Mineral Surfaces in Physics and Chemistry of Mineral Surfaces*; Brady, P. V.; CRC Press: Boca Raton, 1996; pp 1−62.
(11) Deer, W. A.; Howie, R. A.; Zussman, J. *An Introduction to the Rock-forming Minerals*, 2nd ed.; Longman Scientific and Technical: Essex, 1992; pp 1−696.
(12) Bragg, L.; Claringbull, G. F.; Taylor, W. H. *Crystal Structures of Minerals in the Crystalline State*; Bragg, L., Ed.; Cornell University Press: Ithaca, NY, 1965; Vol. IV, p 107.
(13) Oliver, P. M.; Watson, G. W.; Kelsey, E. T.; Parker, S. C. *J. Mater. Chem.* **1997**, *7*, 563.
(14) Ashbee, K. H. G.; Smallman, R. E.; Williamson, G. K. *Proc. R. Soc. A* **1963**, *276*, 542.
(15) Yamada, S.; Tanaka, M. *J. Electron Microscopy* **1997**, *1*, 67.
(16) Lazzeri, M.; Vittadini, A.; Selloni, A. *Phys. Rev. B* **2001**, *63*, 155409.
(17) Kuo, L. Y.; Shen, P. *Mater. Sci. Eng. A* **2000**, *277*, 258.
(18) Shen, P.; Lee, W. H. *Nano Lett.* **2001**, *1*, 707.
(19) Masson, A.; Métois, J. J.; Kern, R. *Surf. Sci.* **1971**, *27*, 463.
(20) Métois, J. J.; Gauch, M.; Masson, A.; Kern, R. *Thin Solid Films* **1972**, *11*, 205.
(21) Métois, J. J. *Surf. Sci*. **1973**, *36*, 269.
(22) Kuo, L. Y.; Shen, P. *Surf. Sci.* **1997**, *373*, L350.
(23) Kern, R.; Masson, A.; Métois, J. J. *Surf. Sci.* **1971**, *27*, 483.
(24) Métois, J. J.; Gauch, M.; Masson, A.; Kern, R. *Surf. Sci.* **1972**, *30*, 43.
(25) Tsai, M. H.; M.S. Thesis, National Sun Yat-sen University, Taiwan 2002.
(26) Jang, H. D.; Friedlander, S. K. *Aerosol Sci. Technol.* **1998**, *29*, 81.
(27) Friedlander, S. K.; Jang, H. D.; Ryu, K. H. *Apply. Phys. Lett.* **1998**, *72*, 173.

NL0495763